

1 *Classification :*
2 SOCIAL SCIENCES: Sustainability Science
3 PHYSICAL SCIENCES: Earth, Atmospheric, and Planetary Sciences
4

5 **Consequences of rapid ice-sheet melting on the** 6 **Sahelian population vulnerability** 7

8 *Author Affiliation:*

9 Dimitri Defrance (1,2), Gilles Ramstein (1), Sylvie Charbit (1), Mathieu Vrac (1), Adjoua Moïse
10 Famien (3,2), Benjamin Sultan (2), Didier Swingedouw (4), Christophe Dumas (1), François
11 Gemenne (5,6), Jorge Alvarez-Solas (7), and Jean-Paul Vanderlinden (5)
12

13 (1) LSCE/IPSL, CEA-CNRS-UVSQ, Université Paris-Saclay, Gif-sur-Yvette, France

14 (2) Sorbonne Universités, UPMC - CNRS-IRD-MNHN, LOCEAN/IPSL, Paris, France

15 (3) LAPA, Université Félix Houphouet Boigny, Abidjan, Côte-d'Ivoire

16 (4) EPOC, Université de Bordeaux, Pessac, France

17 (5) CEARC, OVSQ, Université Paris-Saclay, Guyancourt, France

18 (6) The Hugo Observatory, FNRS, University of Liège, Belgium

19 (7) PalMA Group, Universidad Complutense de Madrid, Madrid, Spain
20

21 *Corresponding Author :*

22 Dimitri Defrance

23 Université Pierre et Marie Curie

24 Boîte 100, 4 place Jussieu

25 75252 Paris Cedex 05

26 France

27 Tel : +33 6 49 49 89 48

28 E-mail : dimitri.defrance@ird.fr
29

30 *Keywords:*

31 climate change ; ice-sheet melting ; impact ; agriculture ; sahel

32 **Abstract**

33 The acceleration of ice sheet melting has been observed over the last few decades. Recent
34 observations and modeling studies have suggested that the ice sheet contribution to future
35 sea level rise could have been underestimated in the latest Intergovernmental Panel on
36 Climate Change report. The ensuing freshwater discharge coming from ice sheets could have
37 significant impacts on global climate, and especially on the vulnerable tropical areas. During
38 the last glacial/deglacial period, megadrought episodes were observed in the Sahel region at
39 the time of massive iceberg surges, leading to large freshwater discharges. In the future, such
40 episodes have the potential to induce a drastic destabilization of the Sahelian agroecosystem.
41 Using a climate modeling approach, we investigate this issue by superimposing on the
42 Representative Concentration Pathways 8.5 (RCP8.5) baseline experiment a Greenland flash
43 melting scenario corresponding to an additional sea level rise ranging from 0.5 m to 3 m. Our
44 model response to freshwater discharge coming from Greenland melting reveals a significant
45 decrease of the West African monsoon rainfall, leading to changes in agricultural practices.
46 Combined with a strong population increase, described by different demography projections,
47 important human migration flows could be potentially induced. We estimate that, without
48 any adaptation measures, tens to hundreds million people could be forced to leave the Sahel
49 by the end of this century. On top of this quantification, the sea level rise impact over coastal
50 areas has to be superimposed, implying that the Sahel population could be strongly at threat
51 in case of rapid Greenland melting.

52 **Significance Statement**

53 A major uncertainty concerning the 21st century climate is the ice sheet response to global
54 warming. Paleodata indicate rapid ice sheet destabilizations during the last deglaciation,
55 which could lead to an underestimation of sea level rise, as suggested in recent publications.
56 Therefore, we explore the impact of different scenarios of Greenland partial melting in the
57 very sensitive Sahel region. We first demonstrate that such a melting induces a drastic
58 decrease of West African monsoon precipitation. Moreover, we quantify the agricultural area
59 losses due to monsoon changes. Consequently, we pinpoint a large potential for migration of
60 millions of people in the coming decades. Thus, the ice sheet destabilization provokes not only
61 coastal damages but also large population migration in monsoon area.

62 The Sahel is particularly exposed to extreme climate variability, as evidenced by the impacts
63 of the severe droughts in the late 20th century (1). Paleoclimatic records have also shown that
64 megadrought episodes occurred in this area during past glacial/deglacial periods (2↓↓↓–5) at
65 the time of huge surges of icebergs (i.e., the so-called Heinrich events), causing outlet glacier
66 acceleration and thus sea level rise (6, 7) (SLR). Several modeling studies performing water-
67 hosing experiments confirmed the close correspondence between the West African monsoon
68 weakening and the freshwater flux (FWF) released to the ocean (8↓↓–10) due to ice sheet
69 melting. These studies raise the question as to whether such episodes could occur during this
70 century in response to a massive freshwater discharge triggered by a significant ice sheet
71 destabilization or surface melting and, if so, what would be the related environmental and
72 human impacts in the Sahel area.

73

74 According to the latest Intergovernmental Panel on Climate Change Fifth Assessment Report
75 (AR5) (11), the likely range of global mean SLR under the Representative Concentration
76 Pathways 8.5 (RCP8.5) scenario is 0.52 m to 0.98 m by the end of the 21st century. Although
77 considerable progress has been made in ice sheet modeling over the last decade, this range is
78 provided with only medium confidence, due to large remaining uncertainties in the ice sheet
79 dynamic response and to an improper representation of the ice–ocean interactions (12).

80

81 In Greenland, recent observations of fjords standing well below sea level suggest important
82 processes of glacier front destabilization (13) that are not included in the current dynamic ice
83 sheet models (14). Moreover, although there are only a few ice shelves surrounding
84 Greenland compared with West Antarctica, post-AR5 remote sensing observations reveal that
85 ice shelves have experienced a continuous thinning for several years, resulting in a buttressing
86 weakening (15, 16), not only in the Antarctic ice sheet but also in Greenland. This leads to a
87 significant ice stream acceleration and possibly to a massive discharge of grounded ice, similar
88 to what occurred during Heinrich events or, more recently, after the collapse of the Larsen B
89 ice shelf (17). Moreover, past episodes of rapid SLR acceleration, such as the Meltwater Pulse
90 1A (18), are still raising questions about our ability to evaluate the future SLR under current
91 understanding of physical mechanisms.

92

93 Results from these past climate studies combined with present-day observations suggest that
94 the ice sheet contribution to SLR could have been underestimated. Here, we consider different
95 freshwater discharge scenarios equivalent to an additional SLR ranging from 0.5 m to 3 m
96 coming from ice sheet melting and/or destabilization, which is not accounted for in the
97 baseline RCP8.5 climate simulation. We explore the related climatic effects on the West
98 African monsoon over the 21st century and their ensuing impacts on the Sahelian cultivable
99 areas and thus on the local population.

100

101 Using the Institut Pierre Simon Laplace low resolution coupled ocean–atmosphere model
102 (IPSL-CM5A-LR) [same version as in the Coupled Model Intercomparison Project, Phase 5
103 (CMIP5) exercise (19); Methods] run under the RCP8.5 radiative forcing from 2006 to 2100,
104 we performed four different water-hosing experiments superimposed to the RCP8.5 scenario
105 in which we added, respectively, a 0.11-, 0.22-, 0.34-, and 0.68-Sv FWF (1 Sv = $10^6 \text{ m}^3\cdot\text{s}^{-1}$)
106 released in the North Atlantic from 2020 to 2070 and corresponding, respectively, to 0.5-, 1-,
107 1.5-, and 3-m SLR. Our goal is, first, to investigate the climatic impacts of the FWF coming from
108 Greenland (GrIS scenarios) in the West African region and, second, to show the impacts on
109 the cereal cultivation in the Sahel area, and the consequences for the local population, which
110 is already facing chronic malnutrition problems.

111 **Changes in tropical precipitation systems**

112 It has been shown that the freshening of the North Atlantic has global climatic impacts (9,
113 20↓↓↓↓–25), including a strong cooling of the Northern Hemisphere down to the Sahara
114 (26↓↓–29) related to a very strong slowdown of the North Atlantic Deep Water (NADW)
115 leading to the slowdown of the Atlantic meridional overturning circulation (AMOC) (9, 20↓↓↓–
116 24). The maximum decrease of the mean annual NADW outflow at 30°N occurs around 2060
117 and corresponds to a reduction of 90% (60%) of the initial NADW value associated with a sea
118 level rise of 3 m (0.5 m) (Fig. 1A). This feature is associated with a large decrease of Sahel
119 rainfall (10% to 60%) between 2030 and 2060 with respect to the RCP8.5 scenario (Fig. 2). This
120 spatial pattern of precipitation changes is similar to the one inferred from the large surge of
121 iceberg discharges that occurred in the past (2, 30). The tropical rainfall changes are linked to
122 the Northern Hemisphere cooling through atmospheric teleconnections. A north–south
123 thermal gradient between the Sahara (cooler) and the Guinea Gulf (warmer) appears (Fig. 1B).
124 This gradient leads to a rise of sea level pressure gradient, inducing low-level southward winds,

125 which block the monsoon system farther south (Fig. 1C). The Sahel becomes drier, and the
126 surface temperature increases; this causes an additional local temperature gradient that
127 strengthens the African Easterly Jet, causing a moisture export from this area (2, 31) (Fig. 1D).
128 These mechanisms underlying the drastic reduction of Sahelian precipitation are robust in
129 different climatic contexts with several models (9, 22).

130 Here we focus on the Western African Sahel region (8°N to 18°N; 17°W to 15°E). Because the
131 Sahelian population is strongly dependent on pastoralism and rainfed agriculture for
132 subsistence (32), our analysis is made in terms of summer precipitation changes [June to
133 September (JJAS)] during which most of the rainfall occurs (between 80% and 90%). To
134 circumvent the acknowledged difficulties of CMIP5 models (33) to properly capture the
135 mesoscale processes and therefore the monsoon rainfall, we applied a statistical method to
136 improve the IPSL simulated precipitation in the West African region with respect to the Water
137 and Global Change project (WATCH) Forcing Data methodology applied to the latest global
138 atmospheric reanalysis data produced by the European Centre for Medium-Range Weather
139 Forecasts (ERA-Interim) (WFDEI) reanalysis (34). This method, called “Cumulative Distribution
140 Function transform” (CDF-t), has been successfully applied in many climate-related studies
141 (e.g., refs. 35–38; Methods).

142

143 To illustrate the internal model variability, we considered a four-member dataset of the
144 RCP8.5 scenario, each member differing in initial conditions. The evolution of the corrected
145 precipitation in the West African Sahel region, obtained under the RCP8.5 dataset (baseline
146 experiments) and the four GrIS scenarios, is displayed in Fig. 3. However, the precipitation
147 signal simulated in response to the 0.5-m SLR perturbation is not statistically significant
148 compared with the four members of the RCP8.5 baseline experiment, as indicated by the t
149 test (P value <0.05; Methods), and the corresponding results will not be further discussed in
150 the following.

151 The effect of the FWF perturbation radically changes the evolution of precipitation averaged
152 over the Sahel region. The first key feature is a significant decrease of Sahel rainfall for the
153 three larger GrIS scenarios (i.e., 1-, 1.5-, and 3-m equivalent SLR) compared with the four-
154 member RCP8.5 dataset. This decrease occurs almost concomitantly with the FWF release and
155 can be up to 30% over the period 2030–2060, reaching 3 mm·d⁻¹, where the greatest
156 differences with the baseline experiment scenario are simulated (P value <0.05). When the

157 freshwater perturbation stops, P_{av} increases slightly, and values close to those of the baseline
158 experiment are recovered.

159 **Increasing vulnerability**

160 The Sahelian agroecosystem is likely to be strongly disturbed by these large precipitation
161 changes; this could have significant impacts on populations extremely dependent upon
162 rainfed agriculture for subsistence. It is documented that the rainfall decrease and the
163 temperature elevation in the Sahel will negatively impact yields of staple food cereals, such as
164 sorghum and millet (39). The water demand for these crops is calculated by Food and
165 Agriculture Organization (FAO) formulations (Methods) and depends on temperature. The
166 north–south gradient of water demand has a similar amplitude for sorghum and millet,
167 directly related to the temperature gradient. In the Sahel area, the sorghum needs, currently,
168 between 520 mm and 660 mm per growing period. The millet growth period is shorter than
169 that of sorghum and needs therefore less water (460 mm to 600 mm per growing period). The
170 water demand increases over the 21st century, due to the temperature increase. In average
171 on the Sahel area, the water demand values rise from 580 mm (515 mm) to 650 mm (580 mm)
172 per growing period for the sorghum (millet).

173
174 To quantify the impacts of rainfall decrease on the population, we analyze the gain or loss of
175 available area for agriculture relative to the adequacy between the sorghum water
176 requirement and the JJAS precipitation. Fig. 4A displays the variations of available area for
177 sorghum cultivation. Under the GrIS scenarios, a strong decrease of the cultivable area with
178 respect to 1976–2005 is observed between 2025 and 2100, up to $\sim 1,100,000$ km² for the 1-
179 m GrIS melting scenario and even more for the 1.5- and 3-m GrIS melting scenarios. After
180 2070, the cultivable area slightly increases, and the RCP8.5 values are progressively recovered,
181 except for the 3-m scenario.

182
183 The large impact of the GrIS scenarios on the local population may be enhanced by a strong
184 demography dynamics in the Sahel. All of the projections of the demography evolution
185 suggest an increase of the population over Africa (40). However, these projections remain
186 uncertain and are strongly dependent on socioeconomic changes that will occur throughout
187 the 21st century (40, 41). To estimate the range of people affected by monsoon variations, we
188 analyze the human impacts related to a loss of cultivable areas for a demography fixed to that

189 of 2011 (lower bound) and for an evolving demography deduced from a shared socioeconomic
190 pathway (41) (SSP3 hereafter), which is consistent with the RCP8.5 scenario (upper bound).

191

192 Considering the Sahelian population fixed to its 2011 level (i.e., 135 million people, Fig. 4B),
193 the GrIS scenarios lead to a rapid growth (in less than 20 y) of people impacted by the loss of
194 cultivable area, up to ~60 million people in the 1.5- and 3-m GrIS melting scenarios between
195 2040 and 2065, due to change in precipitation regimes. This number slightly decreases at the
196 end of the FWF perturbation. However, the most dramatic consequences are observed when
197 the population dynamics are accounted for (Fig. 4C). According to the SSP3 scenario, the
198 number of people living below the water threshold (Methods) for sorghum cultivation
199 undergoes a rapid and continuous increase, up to ~360 million by the end of the 21st century.
200 This number represents one third of the population living in the Sahel area, showing that the
201 climatic impact is widely amplified by the demography explosion. This situation will put a
202 considerable strain on millet and sorghum subsistence agriculture. For local farmers,
203 migration might thus appear as a necessary option, especially if one considers the rapid
204 development of African metropolises. Options are, indeed, likely to be limited for local
205 farmers, and staying on their land would require substantial changes in agricultural techniques
206 and the abandonment of subsistence agriculture (42).

207

208 We demonstrated that Greenland melting during the 21st century could drastically affect the
209 climate, not only in high-latitude locations but also over the tropical areas, through
210 atmospheric and oceanic teleconnections. Although most studies focus on the coastal impacts
211 of SLR (43), we pointed out that Greenland melting could produce drastic droughts in the
212 Sahel, with many consequences for agricultural practices and for population migrations. In the
213 past, monsoon-dependent farmers have used the cities (44) and the coastal zones as a refuge
214 or a final migration destination following rainfall deficit years. Under the 1-m SLR scenario or
215 one involving higher SLR, coastal zones will be extremely destabilized, and migration to these
216 regions will be difficult, with a possible “coastal squeeze” (45), making the urban areas the
217 primary destination for migrants. Today, most migrant flows related to environmental
218 disruptions occur within their national or regional boundaries (46). A rapid melting of ice
219 sheets, however, is likely to lead to dramatic population shifts that would develop beyond
220 borders and would entail irreversible demographic impacts.

221 **Methods**

222

223 **Model and experimental details**

224

225 **Model and Experimental Details**

226 All of the experiments presented in this study have been carried out with the coupled
227 atmosphere–ocean IPSL-CM5A-LR model (19), which has been used for the CMIP5 exercise.
228 The atmospheric component has a spatial resolution of $3.75^\circ \times 1.875^\circ$ in longitude and
229 latitude, respectively, with 39 vertical levels; the oceanic component uses an irregular grid
230 with a nominal resolution of 2° , and a higher latitudinal resolution of 0.5° in the equatorial
231 ocean, and 31 vertical levels. The locations of freshwater inputs have been designed to
232 produce a rapid response of the model. We therefore chose to release the freshwater in
233 locations of deep water formations, in the North Atlantic (45°N to 65°N , 45°W to 5°E), which
234 also coincides with regions of input of Greenland meltwater (47). Recent papers pointed out
235 relationships between Greenland melting and AMOC variations (48). The spread of FWF values
236 (0.11 Sv to 0.68 Sv) has been chosen to explore the impact of a large and rapid freshwater
237 input due to partial melting of the Greenland ice sheet. The highest FWF (0.68 Sv) accounts
238 for the fact that current climate models are possibly too stable in response to freshwater
239 release (49). A growing number of modeling results support this assumption by invoking (i)
240 intrinsic model biases in advection (50–54) and/or in the stratification of the subpolar gyre
241 (55), (ii) an incorrect representation of freshwater pathways in the absence of an iceberg drift
242 module (10), or (iii) a too coarse resolution of current ocean models that are not eddy-
243 resolving (56, 57). All these factors could potentially lead to a limited sensitivity of projected
244 AMOC to freshwater input. Thus, we analyze here the progressive reduction of the AMOC
245 corresponding to increased FWF and its potential impacts on the Sahelian region. More
246 importantly, moderate scenarios (corresponding to 0.11 Sv to 0.34 Sv) have to be considered
247 regarding the most recent ice sheet observations (e.g., refs. 13, 16, and 58).

248 **Statistical method to adjust the IPSL simulated precipitation**

249 The simulated precipitation have been corrected with respect to the WFDEI reanalyses
250 interpolated to a $0.5^\circ \times 0.5^\circ$ spatial resolution (34), used as a reference. Here, the “calibration”

251 period covers the 34-year time period 1979-2013, while the “projection” period covers the
 252 94-year time period 2006-2099.

253 The bias correction method used in this study is a variant of the “Quantile-Mapping” approach
 254 (e.g., (59, 60)) and allows to account for the climate change signal into the correction (37).
 255 This method called “Cumulative Distribution Function – transform” (CDF-t) was initially
 256 developed by (61) and has then been applied in many climate-related studies (e.g., (35–38),
 257 among others). If X denotes the random variable representing the modelled variable to be
 258 corrected, and Y the random variable representing the reference variable, CDF-t first
 259 estimates the cumulative distributions F_{Yp} and F_{Xp} of the random variables Yp and Xp over
 260 the projection (future) time period before applying a distribution-derived quantile-mapping,
 261 i.e. trying to map a modelled value x_p to a value y_p such that their distributions are equivalent
 262 (62) :

$$263 \quad F_{Yp}(y_p) = F_{Xp}(X_p) \Leftrightarrow y_p = F_{Yp}^{-1}[F_{Xp}(X_p)] \quad (1)$$

264
 265
 266 If F_{Xp} can be directly modelled – parametrically or not – from the data to be corrected in the
 267 projection period, the modelling of F_{Yp} is based on the assumption that a mathematical
 268 transformation T allows going from F_{Xc} to F_{Yc} – the distribution of the random variables Yc
 269 and Xc in the calibration period,

$$270 \quad T[F_{Xc}(z)] = F_{Yc}(z) \quad (2)$$

271
 272 for any z , and that T is still valid in the projection period: that is,

$$273 \quad T[F_{Xp}(z)] = F_{Yp}(z) \quad (3)$$

274
 275 Replacing z by $F_{Xc}^{-1}(u)$ in eq. (2), where u is any probability in $[0, 1]$, we obtain

$$276 \quad T(u) = F_{Yc}[F_{Xc}^{-1}(u)] \quad (4)$$

277
 278 corresponding to a simple definition for T . Inserting eq. (4) in eq. (3) leads to a modelling of
 279 F_{Yp} :

$$280 \quad F_{Yp}(z) = F_{Yc} \left[F_{Xc}^{-1} [F_{Xp}(z)] \right] \quad (5)$$

281

282 Once F_{Xp} and then F_{Yp} are modelled, a distribution-based quantile-mapping is applied as in
283 eq. (1). Hence, this CDF-t approach includes the information about the distributions over the
284 projection time period in the quantile-mapping technique. More details can be found in (37).

285 To refine the bias correction method, a multivariate mapping could be performed, notably to
286 better account for effect of the meso-scale processes (e.g. AEJ instabilities giving rise to squall
287 lines) that could counteract those of the large-scale circulation. Such a multivariate approach
288 would require wind data in altitude that are not currently available. Moreover, multivariate
289 statistical bias correction methods are only emerging in the literature and are not yet ready
290 to be used. However, paleoclimatic data reveal that ice-sheet melting produced in the past a
291 strong decrease of the West African monsoon (3–5) with underlying mechanisms fully similar
292 to those highlighted in the present study (2), suggesting that the effect of jet instabilities is
293 insufficient to counterbalance the effect of large-scale circulation (i.e decrease of the
294 monsoon rainfall).

295

296 **t-test for each simulation**

297 To investigate the significance of the monsoon variations due to the freshwater input, we
298 use the t-test. We average the total monsoon precipitation on the Sahel area (8°N-18°N;
299 17°W-15°E) and compare each scenario with the RCP8.5 baseline experiment. The t-test (eq.
300 6) must be done with stationary series:

$$301 \quad t = \frac{\bar{X}_{scen} - \bar{X}_{rcp85}}{\sqrt{\frac{s_{scen}^2}{n_{scen}} + \frac{s_{rcp85}^2}{n_{rcp85}}}} \quad (6)$$

302

303 where:

304 t is the t-test result

305 X is the sample mean for the scenario under study and the RCP8.5 baseline scenarios

306 S^2 is the unbiased estimator of the variance of the two samples

307 n is the number simulated precipitation value in each scenario (i.e 10 for the RCP8.5

308 baseline experiment and 10 for each GrIS scenario)

309 However our scenarios are used in transient experiments. To circumvent this problem, we

310 calculate the t-test values 10 years by 10 years with a time lag of 1 year (i.e. 2006-2015, 2007-

311 2016,...) to obtain 84 pseudo-stationarity periods by subsampling. We obtain a t-value for each
312 year between 2011 and 2094. For each t-test we have, 10 values for one GrIS scenario and 10
313 for the RCP8.5 one, leading to 18 degrees of freedom allowing to have a robust test. A longer
314 period would lead to non-stationarity of our time series and a shorter period to a test with a
315 too large variability, and therefore not usable. Using a probability threshold of 97.5%
316 combined with these 18 degrees of freedom, the critical value is 2.101.

317

318 **Water demand of crops**

319 The threshold of crop water demand evolves with time as a function of temperature: the crops
320 need more water when the temperature increases. The water demand of sorghum cultivation
321 can be obtained for each model grid point in the Sahel area (8°N-18°N; 17°W-15°E). It is
322 estimated with the evapotranspiration (ET₀) given by the Blaney-Criddle technique (63) (eq.
323 7) with a correction factor *kc*, as suggested by the FAO eq. 8 (64), that accounts for specific
324 characteristics of a given crop specie:

$$325 \quad ET_{crop} = kc \times A \quad (7)$$

$$326 \quad ET_0 = p (0.46 T_{mean} + 8) \quad (8)$$

327

328 where:

329 *ET₀* is the potential evapotranspiration (mm/day)

330 *ET_{crop}* is the water demand for crop (mm/growing period)

331 *T_{mean}* = mean temperature over the monsoon period (° C)

332 *A* is the crop growing period duration (i.e 120 days for sorghum, 105 for millet)

333 *p* = percentage of daytime duration.

334 *kc* = crop factor: 0.78 for sorghum, 0.79 for millet

335

336

337 **Surface area and population impacted by rainfall changes**

338 To estimate the variations of the agricultural area due to rainfall changes and the number of
339 inhabitants impacted by the weakening of precipitation, we computed the land surface area
340 receiving an amount of precipitation below the required precipitation threshold for sorghum
341 cultivations. Since the number of inhabitants is given by a 0.5°x0.5° spatial resolution dataset,

342 provided by the Potsdam Institute for Climate Impact Research from a preliminary version of
343 the SSP population data (the 2012-05-11 data in the IIASA database), the rainfall has been bi-
344 linearly interpolated on a 0.5°x0.5° grid. For each scenario (RCP 8.5 and GrIS), the area
345 impacted by rainfall change ($R(t)$) in the Sahel area (8°N-18°N; 17°W-15°E) is obtained year by
346 year with the following equation:

$$347 \quad R(t) = \sum R_{scen}(t) - \sum R_{ref} \quad (9)$$

348

349 where:

350 $R_{scen}(t)$ represents the area covered by the grid points where the precipitation volume
351 is above the water demand of crops

352 R_{ref} represents the area covered by the grid points where the precipitation averaged
353 over the last thirty-year climatic period (1976-2005) is above the water demand of crops.

354

355 To estimate the evolution of the cultivable area affected by a precipitation deficit we express
356 the number of corresponding pixels in km². When the number of pixels is negative (positive),
357 the area available for agriculture is smaller (larger) than that of the 1976-2005 climatic period.
358 The number of inhabitants impacted by rainfall changes is estimated by summing the number
359 of people living in the corresponding surface area. To count only the rural population with
360 only rainfed agriculture practices, the surface area where the current population density is
361 above 200 inhabitants/km² is excluded. A positive (negative) value means that a greater
362 (smaller) number of people is affected by rainfall changes compared to the reference period
363 (1976-2005).

364 **Code and data availability**

365 All data generated in this study by the IPSLCM5A-LR model for the Greenland scenarios as well
366 as and the Ferret and Python scripts produced for their analysis are available from the
367 corresponding author. Other results supporting this study are based on CMIP5 model, WFDEI
368 Re-analysis data and populations projection, which are available
369 respectively from http://cmip-pcmdi.llnl.gov/cmip5/data_portal.html,
370 http://www.eu-watch.org/data_availability and [http://clima-dods.ictp.it/Users/fcolon_g/ISI-](http://clima-dods.ictp.it/Users/fcolon_g/ISI-MIP/)
371 [MIP/](http://clima-dods.ictp.it/Users/fcolon_g/ISI-MIP/).

372 **Acknowledgements**

373 We thank Michel Crucifix and an anonymous reviewer for their constructive comments
374 and suggestions that helped improve the manuscript, as well as Serge Janicot and Juliette
375 Mignot for fruitful discussions. We are also very grateful to Sarah Amram, Jean-Yves
376 Peterschmitt, and Aurélien Quiquet for technical support, and to Sandra Bouneau and
377 Sylvain David for numerous exchanges. This work was supported by the French Atomic
378 Commission (CEA) within the framework of the Variations Abruptes du Climat:
379 Conséquences et Impacts éNergétiques project funded by the Département des sciences
380 de la matières (DSM) with the DSM-Energie Program. It benefited from the high
381 performance computing (HPC) resources made available by Grand Equipement National
382 de Calcul Intensif, CEA, and Centre National de la Recherche Scientifique. The authors
383 thank the Potsdam Institute for Climate Impact Research for providing the gridded data
384 population (SSP3) based on a preliminary version of the SSP population data (the 2012-
385 05-11 data in the IIASA database). This database has been elaborated within the Inter-
386 Sectoral Impact Model Intercomparison Project.

387

388 **References**

- 389 1. Hulme M, Doherty R, Ngara T, New M, Lister D (2001) African climate change: 1900-2100. *Clim*
390 *Res* 17(2):145–168.
- 391 2. Mulitza S, et al. (2008) Sahel megadroughts triggered by glacial slowdowns of Atlantic
392 meridional overturning. *Paleoceanography* 23(4):PA4206.
- 393 3. Stager JC, Ryves DB, Chase BM, Pausata FSR (2011) Catastrophic drought in the Afro-Asian
394 monsoon region during Heinrich event 1. *Science* 331(6022):1299–302.
- 395 4. Itambi AC, Dobeneck T Von, Mulitza S, Bickert T, Heslop D (2009) Millennial-scale northwest
396 African droughts related to Heinrich events and Dansgaard-Oeschger cycles : Evidence in
397 marine sediments from offshore Senegal. 24:1–16.
- 398 5. Tjallingii R, et al. (2008) Coherent high- and low-latitude control of the northwest African
399 hydrological balance. *Nat Geosci* 1(10):670–675.
- 400 6. Broecker W, Bond G, Klas M, Clark E, McManus J (1992) Origin of the northern Atlantic's
401 Heinrich events. *Clim Dyn* 6(3-4):265–273.
- 402 7. Alvarez-Solas J, Robinson A, Montoya M, Ritz C (2013) Iceberg discharges of the last glacial
403 period driven by oceanic circulation changes. *Proc Natl Acad Sci* 110 (41):16350–16354.
- 404 8. Kageyama M, Mignot J (2009) Glacial climate sensitivity to different states of the Atlantic
405 Meridional Overturning Circulation: results from the IPSL model. *Clim Past* 5(3):551–570.
- 406 9. Swingedouw D, et al. (2009) Impact of Freshwater Release in the North Atlantic under
407 Different Climate Conditions in an OAGCM. *J Clim* 22(23):6377–6403.
- 408 10. Swingedouw D, et al. (2013) Decadal fingerprints of freshwater discharge around Greenland in
409 a multi-model ensemble. *Clim Dyn* 41(3-4):695–720.
- 410 11. Church JA, et al. (2013) Sea Level Change. *Climate Change 2013: The Physical Science Basis.*
411 *Contribution of Working Group I to the Fifth Assessment Report of the Intergovernmental*
412 *Panel on Climate Change [Stocker, T.F., D. Qin, G.-K. Plattner, M. Tignor, S.K. Allen, J.*
413 *Boschung, A. Nauels, Y. Xia, pp 1137–1216. Cambridge .*
- 414 12. Straneo F, et al. (2013) Challenges to Understanding the Dynamic Response of Greenland's
415 Marine Terminating Glaciers to Oceanic and Atmospheric Forcing. *Bull Am Meteorol Soc*

- 416 94(8):1131–1144.
- 417 13. Rignot E, Fenty I, Xu Y, Cai C, Kemp C (2015) Undercutting of marine-terminating glaciers in
418 West Greenland. *Geophys Res Lett* 42(14):5909–5917.
- 419 14. Gillet-Chaulet F, et al. (2012) Greenland ice sheet contribution to sea-level rise from a new-
420 generation ice-sheet model. *Cryosph* 6(6):1561–1576.
- 421 15. Paolo FS, Fricker HA, Padman L (2015) Volume loss from Antarctic ice shelves is accelerating.
422 *Science* 348(6232):327–332.
- 423 16. Mouginot J, et al. (2015) Fast retreat of Zachariæ Isstrøm , northeast Greenland. *Science*
424 350(6266):1357–1361.
- 425 17. Alvarez-Solas J, Ramstein G (2011) On the triggering mechanism of Heinrich events. *Proc Natl*
426 *Acad Sci* 108(50):E1359–E1360.
- 427 18. Gomez N, Gregoire LJ, Mitrovica JX, Payne AJ (2015) Laurentide-Cordilleran Ice Sheet saddle
428 collapse as a contribution to meltwater pulse 1A. *Geophys Res Lett* 42(10):3954–3962.
- 429 19. Dufresne J-L, et al. (2013) Climate change projections using the IPSL-CM5 Earth System Model:
430 from CMIP3 to CMIP5. *Clim Dyn* 40(9-10):2123–2165.
- 431 20. Manabe S, Stouffer RJ (1988) Two Stable Equilibria of a Coupled Ocean-Atmosphere Model. *J*
432 *Clim* 1(9):841–866.
- 433 21. Vellinga M, Wood RA, Gregory JM (2001) Processes Governing the Recovery of a Perturbed
434 Thermohaline Circulation in HadCM3. *J Clim* 15:764–780.
- 435 22. Stouffer R, Yin J, Gregory J (2006) Investigating the causes of the response of the
436 thermohaline circulation to past and future climate changes. *J Clim* 19(8):1365–1387.
- 437 23. Kageyama M, et al. (2013) Climatic impacts of fresh water hosing under last glacial Maximum
438 conditions: A multi-model study. *Clim Past* 9(2):935–953.
- 439 24. Jackson R, et al. (2015) Global and European climate impacts of a slowdown of the AMOC in a
440 high resolution GCM. *Clim Dyn*:3299–3316.
- 441 25. Swingedouw D, Braconnot P, Marti O (2006) Sensitivity of the Atlantic Meridional Overturning
442 Circulation to the melting from northern glaciers in climate change experiments. 33(April):1–
443 4.
- 444 26. Peterson LC, Haug GH, Hughen KA, Röhl U (2007) Tropical Atlantic During the Last Glacial
445 Rapid Changes in the Hydrologic Cycle of the Tropical Atlantic During the Last Glacial. *Science*
446 (80-). doi:10.1126/science.290.5498.1947.
- 447 27. Leduc G, et al. (2007) Moisture transport across Central America as a positive feedback on
448 abrupt climatic changes. *Nature* 445(7130):908–11.
- 449 28. Chiang JCH, Bitz CM (2005) Influence of high latitude ice cover on the marine Intertropical
450 Convergence Zone. *Clim Dyn*. doi:10.1007/s00382-005-0040-5.
- 451 29. Arbuszewski J a., deMenocal PB, Cléroux C, Bradtmiller L, Mix A (2013) Meridional shifts of the
452 Atlantic intertropical convergence zone since the Last Glacial Maximum. *Nat Geosci*.
453 doi:10.1038/ngeo1961.
- 454 30. Niedermeyer EM, et al. (2009) Extratropical forcing of Sahel aridity during Heinrich stadials.
455 *Geophys Res Lett* 36:L20707.
- 456 31. Liu Y, Chiang JCH, Chou C, Patricola CM (2014) Atmospheric teleconnection mechanisms of
457 extratropical North Atlantic SST influence on Sahel rainfall. *Clim Dyn* 43(9-10):2797–2811.

- 458 32. Ickowicz A, et al. (2012) Crop-Livestock Production Systems in the Sahel - Increasing Resilience
459 for Adaptation to Climate Change and Preserving Food Security. *Building Resilience for*
460 *Adaptation to Climate Change in the Agriculture Sector*, pp 261–294.
- 461 33. Christensen JH, et al. (2013) Climate Phenomena and their Relevance for Future Regional
462 Climate Change. *Climate Change 2013: The Physical Sci - Ence Basis. Contribution of Working*
463 *Group I to the Fifth Assessment Report of the Intergovernmental Panel on Climate Change*
464 [*Stocker, T.F., D. Qin, G.-K. Plattner, M. Tignor, S.K. Allen, J. Boschung, A. Nauels, Y. X.*]
- 465 34. Weedon GP, et al. (2014) The WFDEI meteorological forcing data set: WATCH Forcing Data
466 methodology applied to ERA-Interim reanalysis data. *Water Resour Res* 50(9):7505–7514.
- 467 35. Oettli P, Sultan B, Baron C, Vrac M (2011) Are regional climate models relevant for crop yield
468 prediction in West Africa? *Environ Res Lett* 6(1):14008.
- 469 36. Colette A, Vautard R, Vrac M (2012) Regional climate downscaling with prior statistical
470 correction of the global climate forcing. *Geophys Res Lett* 39(13):L13707.
- 471 37. Vrac M, et al. (2012) Dynamical and statistical downscaling of the French Mediterranean
472 climate: uncertainty assessment. *Nat Hazards Earth Syst Sci* 12(9):2769–2784.
- 473 38. Vigaud N, Vrac M, Caballero Y (2013) Probabilistic downscaling of GCM scenarios over
474 southern India. *Int J Climatol* 33(5):1248–1263.
- 475 39. Sultan B, et al. (2013) Assessing climate change impacts on sorghum and millet yields in the
476 Sudanian and Sahelian savannas of West Africa. *Environ Res Lett* 8(1):014040.
- 477 40. KC S, Lutz W (2014) The human core of the shared socioeconomic pathways: Population
478 scenarios by age, sex and level of education for all countries to 2100. *Glob Environ Chang.*
479 doi:10.1016/j.gloenvcha.2014.06.004.
- 480 41. O’Neill BC, et al. (2014) A new scenario framework for climate change research: the concept
481 of shared socioeconomic pathways. *Clim Change* 122(3):387–400.
- 482 42. Juana JS, Kahaka Z, Okurut FN (2013) Farmers’ Perceptions and Adaptations to Climate
483 Change in Sub-Sahara Africa: A Synthesis of Empirical Studies and Implications for Public
484 Policy in African Agriculture. *J Agric Sci* 5(4):121–135.
- 485 43. Neumann B, Vafeidis AT, Zimmermann J, Nicholls RJ (2015) Future Coastal Population Growth
486 and Exposure to Sea-Level Rise and Coastal Flooding - A Global Assessment. *PLoS One*
487 10(3):e0118571.
- 488 44. Afolayan AA, Adelekan IO (1999) The role of climatic variations on migration and human
489 health in Africa. *Environmentalist* 18(4):213–218.
- 490 45. Pontee N (2013) Defining coastal squeeze: A discussion. *Ocean Coast Manag* 84:204–207.
- 491 46. McLeman R a., Hunter LM (2010) Migration in the context of vulnerability and adaptation to
492 climate change: Insights from analogues. *Wiley Interdiscip Rev Clim Chang* 1(3):450–461.
- 493 47. Bamber J, van den Broeke M, Ettema J, Lenaerts J, Rignot E (2012) Recent large increases in
494 freshwater fluxes from Greenland into the North Atlantic. *Geophys Res Lett* 39(19):L19501.
- 495 48. Rahmstorf S, et al. (2015) Exceptional twentieth-century slowdown in Atlantic Ocean
496 overturning circulation. *Nat Clim Chang* 5(5):475–480.
- 497 49. Valdes P (2011) Built for stability. *Nat Geosci* 4(7):414–416.
- 498 50. Liu W, Liu Z, Brady EC (2014) Why is the AMOC monostable in coupled general circulation
499 models? *J Clim* 27(6):2427–2443.

- 500 51. Liu W, Xie S, Liu Z, Zhu J (2017) Overlooked possibility of a collapsed Atlantic Meridional
501 Overturning Circulation in warming climate. *Sci Adv* 3(January):e1601666.
- 502 52. Deshayes J, et al. (2013) Oceanic hindcast simulations at high resolution suggest that the
503 Atlantic MOC is bistable. *Geophys Res Lett* 40(12):3069–3073.
- 504 53. Hofmann M, Rahmstorf S (2009) On the stability of the Atlantic meridional overturning
505 circulation. *Proc Natl Acad Sci U S A* 106(49):20584–20589.
- 506 54. Weber SL, et al. (2006) The modern and glacial overturning circulation in the Atlantic ocean in
507 PMIP coupled model simulations. *Clim Past Discuss* 2(5):923–949.
- 508 55. Sgubin G, Swingedouw D, Drijfhout SS, Mary Y, Bennabi A (2017) Abrupt cooling over the
509 North Atlantic in modern climate models. *Nat Commun* 8:14375.
- 510 56. Spence P, Saenko OA, Sijp W, England MH (2013) North Atlantic Climate Response to Lake
511 Agassiz Drainage at Coarse and Ocean Eddy-Permitting Resolutions. 2651–2667.
- 512 57. Weijer W, Maltrud ME, Hecht MW, Dijkstra HA, Kliphuis MA (2012) Response of the Atlantic
513 Ocean circulation to Greenland Ice Sheet melting in a strongly-eddy ocean model.
514 39(May):1–6.
- 515 58. Noël B, et al. (2017) A tipping point in refreezing accelerates mass loss of Greenland’s glaciers
516 and ice caps. 8:14730.
- 517 59. Déqué M (2007) Frequency of precipitation and temperature extremes over France in an
518 anthropogenic scenario: Model results and statistical correction according to observed values.
519 *Glob Planet Change* 57(1):16–26.
- 520 60. Gudmundsson L, Bremnes JB, Haugen JE, Engen-Skaugen T (2012) Technical Note:
521 Downscaling RCM precipitation to the station scale using statistical transformations—a
522 comparison of methods. *Hydrol Earth Syst Sci* 16(9):3383–3390.
- 523 61. Michelangeli P, Vrac M, Loukos H (2009) Probabilistic downscaling approaches: Application to
524 wind cumulative distribution functions. *Geophys Res Lett* 36(11):L11708.
- 525 62. Panofsky HA, Brier GW (1958) *Some applications of statistics to meteorology* (Mineral
526 Industries Extension Services, College of Mineral Industries, Pennsylvania State University).
- 527 63. Blaney HF, Criddle WD (1965) Determining Water Requirements For Settling Water Disputes.
528 *Nat Resour J* 4(1938):29–41.
- 529 64. FAO (2016) 2. Water and soil requirements. Available at:
530 <http://www.fao.org/docrep/u3160e/u3160e04.htm>.
- 531
- 532

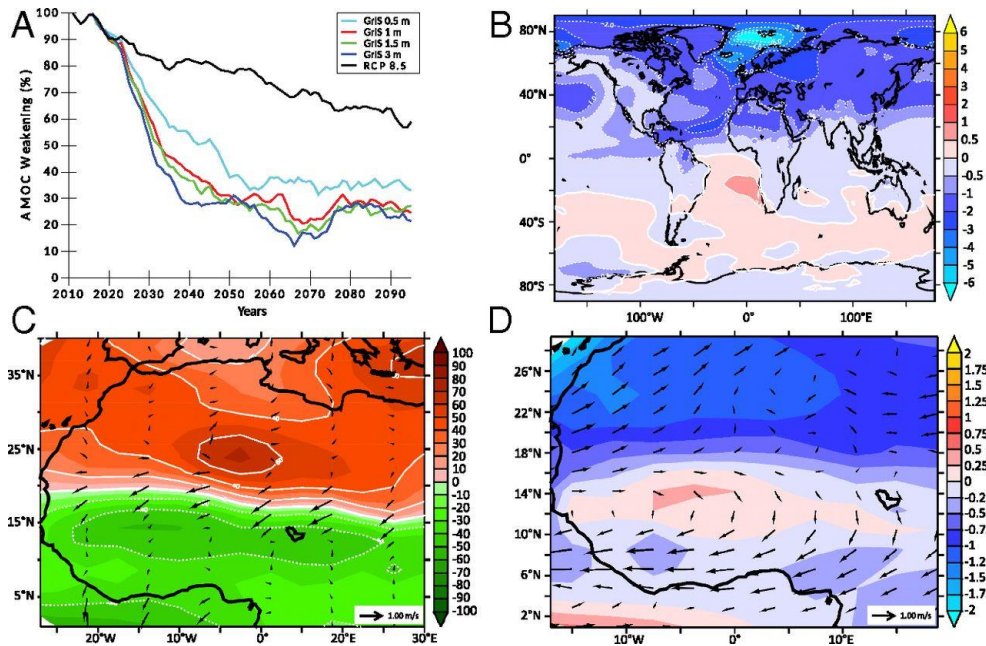


Figure 1: Teleconnection mechanisms linking the Greenland ice sheet melting and the decrease of the Sahelian rainfall. A) AMOC evolution (in % with respect to the present-day values); B) Mean annual temperature anomaly between the 1.5 m GrIS and the RCP8.5 scenarios averaged over the period 2030-2060; C) Same as B) for the sea-level pressure anomaly; and the 10-m winds (black arrows); D) Same as B) for the mean summer (JJAS) temperature anomaly and the 850 hPa winds (black arrows).

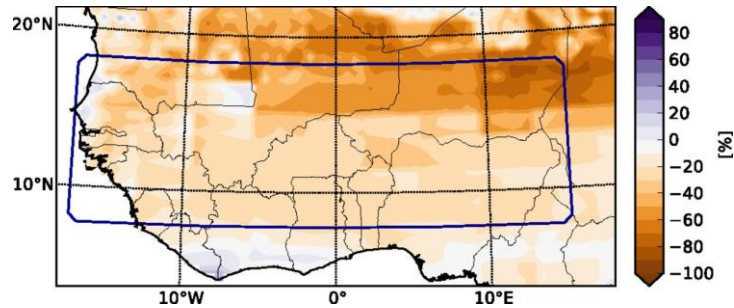


Figure 2: JJAS precipitation anomaly between the 1.5 m GrIS scenario and the RCP 8.5 baseline experiment normalized to the RCP 8.5 values and averaged over 2030-2060. A value of 100 corresponds to a doubling of precipitation and -100 corresponds to zero precipitation. The precipitation values are obtained after applying the statistical method (see Methods). The blue box (8°N-18°N , 17°W-15°E) represents the region under study.

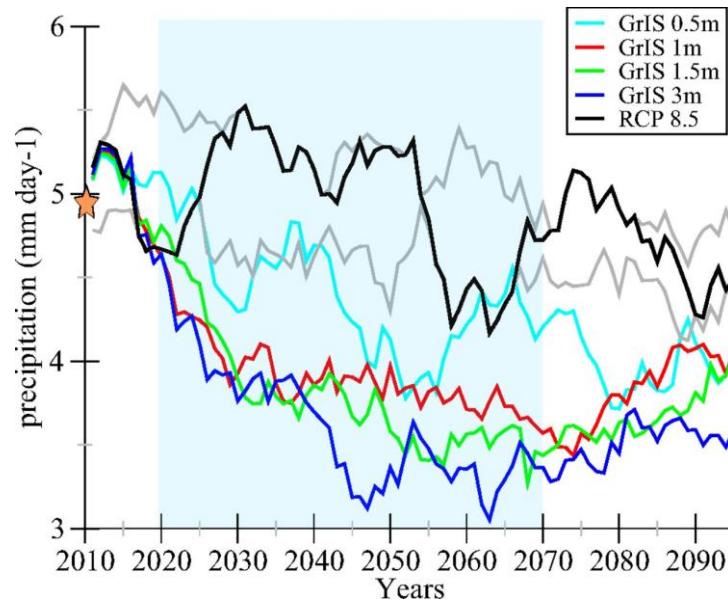
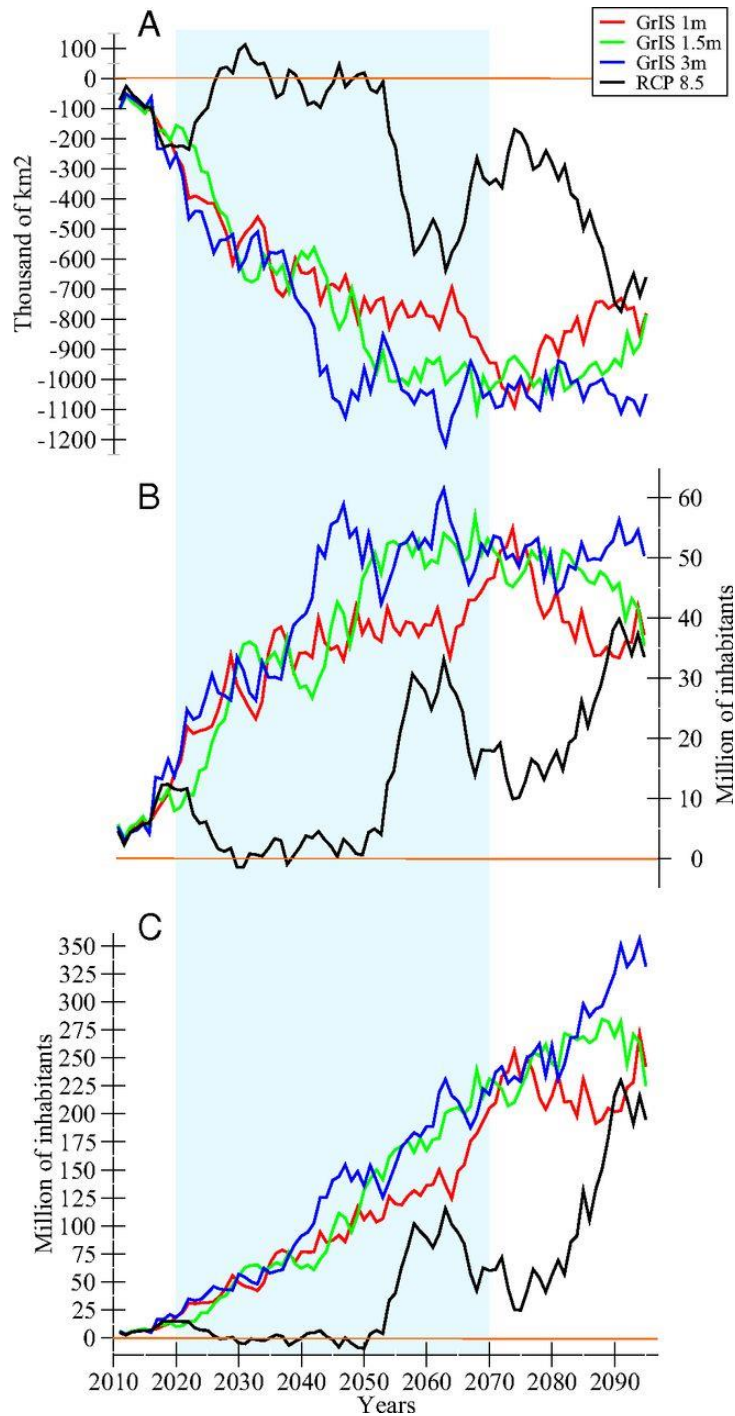


Figure 3: Evolution of JJAS precipitation during the 21st century averaged over the Sahel area (8°N-18°N, 17°W-15°E) for the RCP8.5 and the GrIS scenarios. The orange star indicates the simulated JJAS precipitation over the climatic reference period (1976-2005) deduced from the IPSL-CM5A simulated precipitation (4.96 mm). To illustrate the internal model variability, we considered a 4-member dataset of the RCP8.5 scenario, each member differing in initial conditions. The area delimited by the two grey curves represents the range of model variability deduced from the 4-member dataset.



534

Figure 4: Impacts of rainfall change on sorghum cultivation and on population. A) Evolution of the surface area available for sorghum cultivation (i.e. when the average JJAS precipitation is above the sorghum water demand) for each GrIS scenario and for the baseline experiment. The evolution of the available cultivable area is given with respect to the available area averaged over the 1976-2005 reference period deduced from the historical IPSL-CM5A simulated precipitation. Negative (positive) values indicate a loss (gain) of cultivable area; B) Evolution of the number of inhabitants living under the sorghum water demand with respect to the 1976-2005 historical reference period. This evolution is estimated with the assumption that the number of inhabitants is fixed to its 2011 level; C) Evolution of the number of inhabitants living under the sorghum water demand with respect to the 1976-2005 historical reference period. Here, this evolution accounts for the evolution of demography provided by the SSP3 scenario. Both in (B) and (C), positive values indicate that the number of inhabitants living under the sorghum water demand increases with respect to the reference period.